Prediction of Delamination Onset and Critical Force in Carbon/Epoxy Panels Impacted by Ice Spheres

Jennifer D. Rhymer[1]**, Hyonny Kim**[1]

Abstract: Polymer matrix composite structures are exposed to a variety of impact threats including hail ice. Internal delamination damage created by these impacts can exist in a form that is visually undetectable. This paper establishes an analysis methodology for predicting the onset of delamination damage in toughened carbon/epoxy composite laminates when impacted by high velocity ice spheres (hailstones). Experiments and analytical work focused on ice sphere impact onto composite panels have determined the failure threshold energy as a function of varying ice diameter and panel thickness, and have established the ability to predict the onset of delamination using cohesive elements in explicit dynamic finite element analysis. A critical force associated with damage onset was found to be independent of the ice diameter and thus can be expressed as a function of basic panel-describing parameters, namely bending rigidity and interlaminar fracture energy. Critical force can be used as a failure criterion in simpler models (e.g., shell elements) when predicting the onset of delamination by high speed spherical ice impact.

Keywords: Ice impact, hail, composite, delamination prediction, cohesive zone, critical force

1   Introduction

Lightweight composite structures are vulnerable to being damaged when subjected to impact loading. For aircraft structures, hail ice is of great interest due to the large area over which impacts from hail can occur: all upper and side-facing surfaces are exposed to falling "ground" hail, while all forward-facing surfaces exposed to impact at in-flight speeds. Examples of aircraft structures susceptible to hail impact damage include the fuselage, wings, empennage, radomes, and nacelles. Due to its crushing nature, an ice projectile can produce internal damage, particularly delamination and stiffener-skin separation, without leaving any externally visible

---

[1] Dept. of Structural Engineering, University of California San Diego, La Jolla, CA 92093 USA

indications (namely dents and cracks) of the presence of damage. The prediction of non-visible internal damage, such as delamination, is of particular interest, as the onset of the formation of impact damage can be associated with the impact damage resistance of a structure. Such prediction capability assists in the making of decisions related to skin thickness sizing such that the skin is resistant to damage from a known level of impact threat (e.g., ice diameter and velocity).

Impact damage formation in composites has been extensively studied, with a large body of work focused on low velocity impact. The work of Davies and Zhang (1995) as well as Schoeppner and Abrate (2000) serve as key examples, where instrumented tests measured force history information during impact, and the dependency of damage formation was related to panel thickness. Both works focused on the existence of a critical threshold force which served as a key parameter describing when damage initiation occurred. These tests were performed by the use of low velocity high mass drop weight systems with instrumented (force measuring) metallic impactors that are essentially non-deforming relative to the composite panel response.

A significant difference between the classification of high vs. low velocity impact regimes was explained by authors Jackson and Poe (1992). They highlighted the different force response of impacted structures over a wide range of speeds, from quasi-static-like large mass impact to high speed dynamic small mass impact. Specifically, dynamic small mass impact event occurs with sufficiently high velocity such that the impactor-to-target contact time was very short, during which the initial target response was wave dominated and therefore independent of boundary conditions. Large mass impact events, being much slower, have been shown to behave similarly to quasi-static indentations [Jackson and Poe (1992)] and thus they were strongly influenced by boundary conditions. Olsson (2010) explains that for low velocity or large mass impacts, the peak load and peak deflection are co-incident, while for high velocity or small mass impacts, the peak load occurs very quickly as the panel deflection continues to increase over a much larger time scale.

Force is considered to be a critical parameter in understanding impact events [Jackson and Poe (1992)]. However, it is not possible to directly measure the impact contact force history of simulated hail ice (SHI) impacts onto flexible targets (composite panels) without disrupting the natural response of the target. This is due to the inherent nature of the high speed crushing ice projectile. It should be noted that the term SHI is used to distinguish between laboratory-made cast ice spheres (water frozen into spherical shape) and naturally-occurring hailstones which have a complex layered structure with each layer often being of varying density (porosity). Therefore, this work examines the impact of high velocity SHI onto composite laminates including the numerical simulation-based prediction of the contact force

history and experimentally-measured damage initiation threshold.

Previous works by Kim and Kedward (2000); Kim, Welch and Kedward (2003); Rhymer and Kim (2010) investigating ice impact onto composites have established failure threshold energy (FTE) values (projectile kinetic energy related to onset of damage formation) for thin woven carbon/epoxy panels and created a first-generation finite element analysis (FEA) model of the ice projectile [Kim and Kedward (2000)]. More recent improvements to the FEA ice material model incorporated strain rate dependent strength effects [Tippmann, Kim and Rhymer (2013)] which provides an ice sphere impact model requiring no additional user-tuned input. The material properties and failure response of the SHI model are essential to the accurate simulation of ice impact events because the ice behavior controls the interaction of the impacting projectile onto the composite panel target, and therefore the contact force and internal stress development. The use of FEA to determine the force history for ice impact has been implemented previously by Kim and Kedward (2000) as well as by Juntikka and Olsson (2009) and Olsson and Juntikka (2010). The prior work by Kim and Kedward (2000) modeled the target panels with elastic-only response, however, and did not establish the capability to determine the onset of impact-induced damage.

This present work establishes the ability to predict the onset of delamination damage from ice impact using explicit dynamic FEA models which incorporate cohesive elements between layers of solids. Prediction of the onset of delamination damage (i.e., the damage threshold) allows one to predict a composite structure's damage resistance against the hail ice impact threat. In addition to allowing one to determine suitable skin thickness so that a structure can withstand expected ice impact threat levels, such prediction capability also assists in the determination of when and where focused inspections are needed following an ice impact event. The model described herein does not require tuning (i.e., material parameters not adjusted to match experiments) and has been shown to match with experimental data. Numerical results enabled a deeper understanding of the experiments, allowing the observation that a key parameter defining damage onset is critical force, i.e., a threshold level of contact force at which damage onset occurs. While other papers have suggested critical force as a key parameter [Olsson (2010)], the current work uses experiments and numerical analysis to substantiate this claim specifically for ice impacts. Critical threshold force is of interest since it establishes a simpler criterion by which the initiation of damage can be predicted.

2 Experiments

A series of experiments were previously conducted by Rhymer and Kim (2010); Rhymer, Kim and Roach (2012), focused on determining the FTE of SHI impact-

ing composite panels. The FTE is defined as the minimum amount of incoming projectile kinetic energy required to initiate damage (typically delamination) in the structure. The FTE was found by conducting many impact tests onto composite panels, over a wide range of projectile kinetic energy, to determine at what kinetic energy level delamination (or other initial damage modes) started to occur. The testing and results have been previously presented in detail by Rhymer and Kim (2010); Rhymer, Kim and Roach (2012) and thus only a brief summary is included herein.

Table 1: T800/3900-2 Lamina Material Properties [Tong and Soutis (2003)]

Young's Modulus:	
$E_{11}(GPa)$	160
$E_{22}(GPa)$	8.97
$E_{33}(GPa)$	8.97
Poisson's Ratio:	
v_{12}	0.28
v_{13}	0.28
v_{23}	0.36
Shear Modulus:	
$G_{12}(GPa)$	6.21
$G_{13}(GPa)$	6.21
$G_{23}(GPa)$	3.45
Density:	
$\rho(kg/m^3)$	2700
Strength:	
Longitudinal Tensile (*MPa*)	2843
Longitudinal Compressive (*MPa*)	1553
Transverse Compressive (*MPa*)	166

Actual naturally occurring hailstones were not readily available for experimentation and therefore simulated hail ice (i.e., cast frozen water) spheres were used and are referred to as SHI to distinguish it from natural hail ice. For this study, three sizes of SHI were considered: 38.1, 50.8, and 61.0 *mm* diameter. These sizes of SHI were used to impact composite panels of 304 *mm* square dimension, and of three thicknesses: 8 plies (1.59 *mm*), 16 plies (3.11 *mm*), and 24 plies (4.66 *mm*). All lay-ups were quasi-isotropic, specifically: $[0/45/90/-45]_S$, $[0/45/90/-45]_{2S}$, and $[0/45/90/-45]_{3S}$. These panels were made from the Toray T800/3900-2 carbon/epoxy unidirectional tape (Boeing specification BMS8-276N) material system.

The carbon/epoxy plies were 0.195 *mm* thick and the material properties (obtained from the open literature [Tong and Soutis (2003)]) are summarized in Table 1. Additionally, a thin (0.05 *mm*) plain weave fabric Toray glass/epoxy layer (Boeing specification BMS8-331) was located on the impact side to represent aircraft skin construction practices where the glass/epoxy fabric serves as a protective outer surface ply.

The SHI were launched to desired velocity using the gas gun shown in Figure 1a. The ice was placed into a split rigid urethane foam sabot to protect it from damage (and melting upon contacting the metal barrel) during firing. The sabot aerodynamically separated enough to allow clean release of the ice sphere by the time the sabot was stripped by the sabot stop plate and just the ice sphere passed through the laser photogate velocity measurement system (see Figure 1b). The ice sphere finally impacted the target panel, shown in Figure 1c, which was supported with clamped-type boundary conditions that are defined by a 12.5 *mm* thick steel "picture frame" fixture presenting a 267 *mm* square opening. Each test was observed by a high speed video camera (Phantom v.7.3). The compressed gas (nitrogen or helium) gun has two possible barrel diameter sizes, 79 *mm* and 38 *mm*, which are 2.3 *m* in length. The velocity capability ranges from approximately 30 to 250 *m/sec*. Visual and ultrasonic A-scan (NDT Automation Pocket UT version v1.81 using 5 MHz hand-held probe) inspections were performed after each impact with the panel in the fixture to assess whether or not damage has occurred. This damage information was used in determining the failure threshold of the composite panels.

The high speed video still images in Figure 2a show 61.0 *mm* SHI impacting an 8 ply panel at 65 *m/s*. These images are a typical example of the wave-dominated dynamic response observed in the experiments [Rhymer and Kim (2010); Rhymer, Kim and Roach (2012)] where any impact-induced damage occurring before the main bending wave reaches and returns from the boundaries is not dependent upon the outer boundary conditions. In Figure 2a, the crest of the bending wave can be observed to travel from the panel center to the outer boundaries in roughly 400 μs (for 8 ply panels). Peak contact forces are estimated to develop well before this transit time, before 200 μs, which can be inferred by the correlation between the degree of ice sphere cracking and the time to peak force, as measured for impacts onto the nearly rigid (instrumented) target shown in Figure 2b [Tippmann, Kim and Rhymer (2013)]. For rigid targets, the peak force develops between 50-100 μs after first contact, corresponding to a saturation of new crack growth (occurs between 40 and 80 μs in Figure 2b) and the sphere being broken down into loose debris [Tippmann, Kim and Rhymer (2013)]. Impacts onto flexible targets (i.e., panel) produce lower peak force occurring at a later time (e.g., 200 μs for 8 ply panel in Figure 2a). The FTE measurements reported by Rhymer, Kim and Roach

(a) Gas Gun
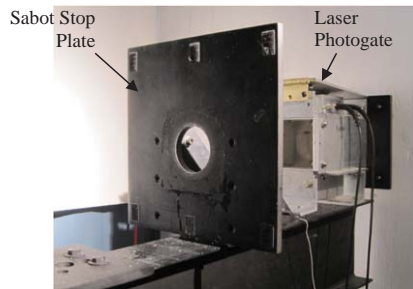
(b) Sabot Stop and Laser Photogate

(c) Composite Panel in Picture Frame Fixture (12.7 mm Steel with 267x267 mm Opening)

Figure 1: High Velocity Impact Testing Equipment

(2012) are therefore applicable to impacts onto composite skins at locations away from internal structural members (e.g., stringers, stiffeners).
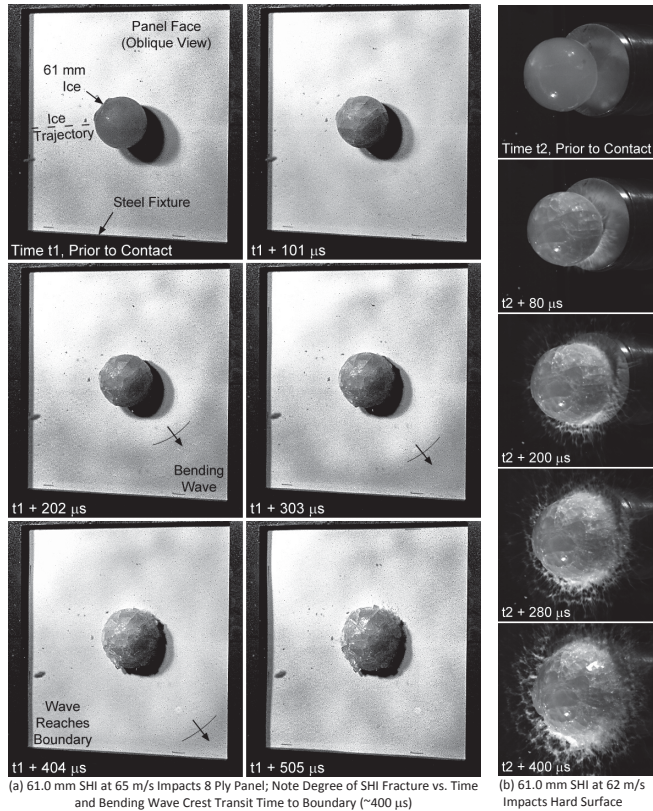

(a) 61.0 mm SHI at 65 m/s Impacts 8 Ply Panel; Note Degree of SHI Fracture vs. Time and Bending Wave Crest Transit Time to Boundary (~400 μs)

(b) 61.0 mm SHI at 62 m/s Impacts Hard Surface

Figure 2: High Speed Video Still Images Comparing Degree of Crushing of 61.0 *mm* SHI Impacting (a) 8 Ply Panel and (b) Nearly Rigid Hard Surface; Times $t_1 < 101\mu s$ and $t_2 < 40\mu s$ Show One Video Frame Just Prior to Contact

A 24 ply panel was instrumented with strain gages to collect data to be used for model validation. Strain gages were attached to the panel center and at 70 *mm* from the center point, in both the zero and 90 degree directions, as shown in Figure 3. The specific strain gages used were Vishay General Purpose 350 Ohm strain gages (L2A-06-250LW-350). The gages were connected to three Vishay 2310B bridge excitation and amplification systems and the data were recorded with an oscilloscope at 5 MHz sampling rate.
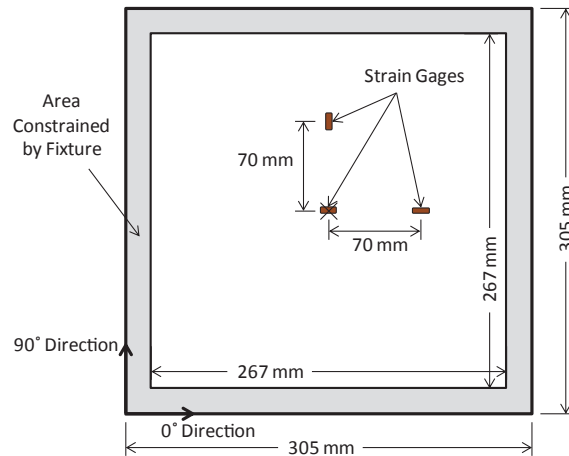
Figure 3: Strain Gage Locations on Instrumented Composite Panels

3 FEA Modeling

The commercial FEA code ABAQUS/Explicit was used to simulate the impact of SHI onto composite panels. The aims of the models were to (i) gain deeper insights from the experiments from contact force and internal stress quantities, and (ii) establish the capability to predict the onset of delamination between plies. The composite panel targets were modeled ply-by-ply with a mesh of hexahedral 8-node reduced integration solid elements (C3D8R in ABAQUS) having orthotropic elastic material properties (no damage) oriented to reflect each carbon/epoxy ply's fiber direction. Since the plain weave glass/epoxy ply on the impact-surface was thin relative to the carbon/epoxy plies (25% of ply thickness), and had much lower elastic modulus (~20%), the glass/epoxy ply stiffness (modulus x thickness) was roughly 20X lower than the carbon/epoxy (in fiber direction) and thus was not included in the model. An example quarter-symmetric mesh for an 8 ply panel impacted by 50.8 *mm* SHI is shown in Figure 4.

Between each layer of panel solid elements (each ply) was a layer of cohesive elements (COH3D8 in ABAQUS), as indicated in Figure 4, which directly predicts delamination onset and growth at any of the ply-to-ply interfaces. Element dimension in the thickness-direction was defined by the ply thickness (0.195 *mm*), while the in-plane dimensions were defined with a 0.98 bias making the elements finer at the impact location. Element size in the in-plane dimension ranged from 0.485 *mm* (at center of plate) to 3.516 *mm* (at boundaries), as shown in Figure 5.

The plan-form mesh shown in Figure 5 having 100×100 elements in the in-plane
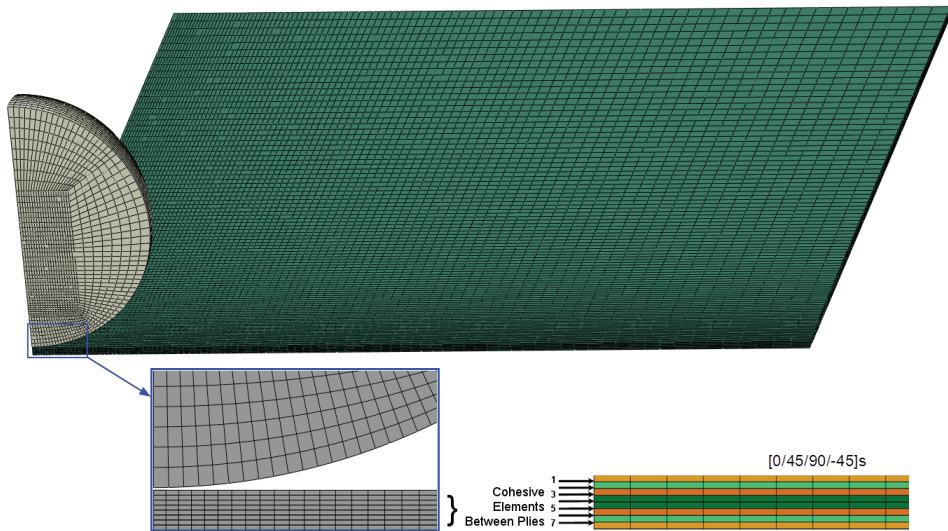
Figure 4: Quarter-Symmetric Mesh for Ply Panel and 50.8 *mm* SHI; Cohesive Element Details
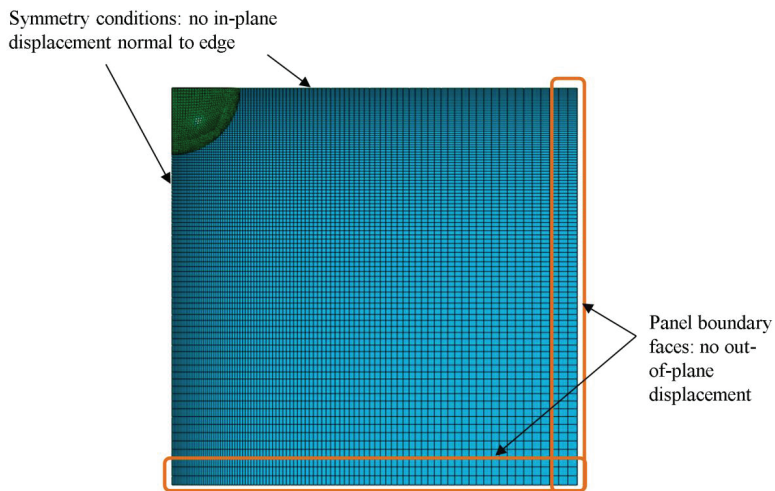

Figure 5: Top View of Panel and SHI Impact, Showing Symmetry Planes and Boundary Condition Areas

directions was used for all panel models (i.e., 8, 16, and 24 plies), with increasing layers of solid elements used to represent more plies. To assess the mesh sensitivity,

the number of in-plane elements was increased to 200×200, with same 0.98 bias (finer at panel center), while keeping the though-thickness element dimension the same. Comparison of the resulting contact force histories was found to be essentially identical, and thus the plan-form mesh refinement level (100×100 elements) was considered adequate for this size target panel. For computational cost reasons, additional through-thickness mesh refinement was not considered as the elements were already quite thin (one ply thickness) in that direction.

A limited series of models were created using shell elements to represent the panel. This was done to investigate the capability of shell elements to predict the contact force developed during impact by SHI so that force a force-based failure criterion can be used for predicting delamination initiation. Shells are much less computationally expensive than the ply-by-ply solid element modeling approach, and are therefore compatible with simulating ice impacts onto large sections of structures. 4-node shell elements (S4 in ABAQUS) were used, with each oriented lamina in the laminate stacking sequence defined by three integration points. Note that the shell models did not incorporate cohesive zone elements and thus did not directly predict delamination onset and growth.
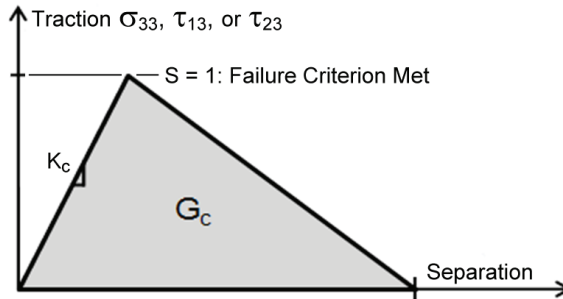

Figure 6: Cohesive Element Traction-Separation Relationship [Dassault Systèmes Simulia Corp (2011)]

The material properties for the composite lamina were obtained from the open literature [Tong and Soutis (2003)], and are listed in Table 1. For the cohesive zone elements located between each layer of solid elements (see Figure 4), the stiffness K_c must be specified which defines the uploading slope for the traction-separation relationship shown in Figure 6. This was chosen to be ten times the stiffness of the surrounding solid elements, as computed by Equation (1),

$$K_c = 10\frac{E_e}{T_e} \tag{1}$$

where E_e and T_e are the Young's modulus and characteristic thickness of the surrounding solid elements. K_c is directly calculated by assuming $E_e = E_{33}$ of the composite (8.97 *GPa* per Table 1) and choosing the characteristic thickness T_e of the surrounding elements to be 0.195 *mm* (one ply thickness). This high stiffness value helps to prevent interpenetration of the plies under intense compressive stress that develops directly under the site of impact contact.

The mass per unit area $\bar{\rho}_c$ of the cohesive elements was calculated by Equation (2) in accordance with ABAQUS user manual [Dassault Systèmes Simulia Corp (2011)] recommendations to minimize the difference in stable time increment between the cohesive zone elements and solid elements.

$$\bar{\rho}_c = \rho_c T_c = 0.1\rho_e T_e \tag{2}$$

In Equation (2), the characteristic thickness of the cohesive elements T_c was set as 1 and thus $\bar{\rho}_c$ can be calculated directly by setting the density of the surrounding elements ρ_e to be the composite material density ($2700 kg/m^3$ per Table 1). The values for K_c and $\bar{\rho}_c$ used in this analysis are given in Table 2.

Table 2: Cohesive Element Model Properties for Interlaminar Fracture [Swanson and Qian (1992); Yokozeki, Ogasawara and Ishikawa (2006); Takeda, Kobayashi, Ogihara and Kobayashi (1999); Davidson and Sediles (2011); Hojo, Matsuda, Tanaka, Ochiai and Murakami (2006)]

Stiffness and Mass Properties:	
Cohesive Element Stiffness, $K_c (TPa/m)$	461.5
Mass Per Unit Area, $\bar{\rho}_c (kg/m^2)$	0.05265
Interlaminar Strengths for Damage Initiation:	
Normal, $\sigma_{33}^{ult} (MPa)$	50
Shear in 1-3 Plane, $\tau_{13}^{ult} (MPa)$	115
Shear in 2-3 Plane, $\tau_{23}^{ult} (MPa)$	115
Critical Strain Energy Release Rates for Damage Evolution:	
Mode I, G_{IC} (J/m2)	710
Mode II, G_{IIC} (J/m2)	2200
Mode III, G_{IIIC} (J/m2)	1700

The cohesive element strength and fracture properties listed in Table 2 were obtained from the open literature [Swanson and Qian (1992); Yokozeki, Ogasawara and Ishikawa (2006); Takeda, Kobayashi, Ogihara and Kobayashi (1999); Davidson and Sediles (2011); Hojo, Matsuda, Tanaka, Ochiai and Murakami (2006)].

The cohesive modeling approach has been shown to be capable of simulating delamination in composites [Gonzalez, Maimi, Turon, Camanho and Renhart (2009); Elmarakbi, Hu and Fukunaga (2009)]. The behavior of these elements was defined by a traction-separation law, shown in Figure 6, with a quadratic stress failure initiation criterion acting on the interlaminar shear (τ_{13} and τ_{23}) and normal (σ_{33}) stress components,

$$S = \left(\frac{\sigma_{33}}{\sigma_{33}^{ult}}\right)^2 + \left(\frac{\tau_{13}}{\tau_{13}^{ult}}\right)^2 + \left(\frac{\tau_{23}}{\tau_{23}^{ult}}\right)^2 = 1 \tag{3}$$

where the interlaminar strengths (denominator terms) are provided in Table 2. When all four integration points in the element reach this stress-based failure initiation criterion, i.e., $S = 1$, the degradation of the cohesive element occurs following the traction-separation relationship (see Figure 6), where the area under the traction-separation curve is equal to the critical strain energy release rate G_c. A power law mixed mode energy damage evolution criterion controlled the delamination growth (cohesive failure),

$$\left(\frac{G_I}{G_{IC}}\right)^{1.5} + \left(\frac{G_{II}}{G_{IIC}}\right)^{1.5} + \left(\frac{G_{III}}{G_{IIIC}}\right)^{1.5} = 1 \tag{4}$$

where G_I, G_{II}, and G_{III} are the strain energy release rates for Mode I, II, and III fracture, respectively, and the "C" subscript denominator terms are the critical interlaminar strain energy release rates for each mode (see values in Table 2).

The ice sphere model development constituted a considerable effort and is documented in detail by Tippmann, Kim and Rhymer (2013), and thus only a brief summary is included herein. The ice sphere was modeled with solid elements and the sphere was meshed with a bias toward the impact side, as shown in Figure 4 (note sphere's mesh finer adjacent to panel). The mesh size and material model for the ice was previously developed by Tippmann, Kim and Rhymer (2013), incorporating strain rate dependent strength within an elastic-plastic definition which included a tensile hydrostatic stress failure criterion. Failed elements behave like a fluid, not being able to carry shear stress but still supporting hydrostatic compression. The ice impact material model has been shown [Tippmann, Kim and Rhymer (2013)] to accurately predict the behavior of ice spheres impacting a rigid target over a wide range of velocity and ice diameter, and here it has been applied to predicting the stresses developed during impact onto flexible composite panels.

The boundary conditions on the panel simulated the "picture frame" steel test fixture, which restricts out-of-plane motion on the outer 19 *mm* of the panel faces, as

shown in Figure 5, but permits in-plane movement. Additionally, the appropriate constraints were applied at the planes of symmetry, and general inclusive contact was specified on all external surfaces. The ice sphere nodes were given a velocity initial condition and the model was run for a long enough duration significantly exceeding the time of peak force, typically between 150 to 500 μs.

4   Results

The impact experiments, described in detail by Rhymer, Kim and Roach (2012), identified the FTE and associated failure threshold velocity (FTV) for each combination of panel thickness and SHI diameter. In order to obtain these threshold values, a series of impact tests were conducted for each condition, and the result of each impact test was described by two parameters: impact energy and damage state. The damage state was restricted to a binary description: zero if no damage occurred and one if damage was detected (by ultrasonic A-scan). In all cases, the initial damage mode was internal delamination with no permanent deformation or other externally-visible indication of damage being present. By plotting the binary damage state (0 or 1) vs. projectile velocity, and employing a logistic regression curve fit, the experimentally-measured FTV values listed in Table 3 were systematically identified [Rhymer, Kim and Roach (2012)].

Table 3: Experimentally-Measured FTV Compared to FEA Predicted FTV and Critical Force

Panel Type (Thickness)	SHI Diameter (*mm*)	FTV Experimental (*m/s*)	FTV FEA (*m/s*)	Percentage Difference	FEA Critical Force (*kN*)
	38.1	115	97.5	-15	9.7
8 ply (1.59 *mm*)	50.8	91	67.5	-26	10.2
	61.0	65	47.5	-27	9.9
	38.1	154	147.5	-4	22.2
16 ply (3.11 *mm*)	50.8	121	107.5	-9	23.2
	61.0	96	82.5	-14	21.4
	38.1	178	N/A*	–	–
24ply (4.66 *mm*)	50.8	154	152.5	-1	44.5
	61.0	127	117.5	-7	42.0

∗Numerical instability caused model termination

FEA models were then used to conduct "numerical experiments" to predict the FTV for each combination of panel thickness and SHI diameter. This activity was conducted independently of the now known experimentally-measured FTV listed in Table 3. First, the overall SHI-to-panel interaction and panel deformation response were compared (see Figure 7) between the FEA and experimental observations. Figure 7 shows the 38.1 *mm* SHI locally crushing onto the panel face

(reflective black surface in left-hand images is carbon/epoxy panel) during the first 100 microseconds after initial contact. The FEA correctly predicts the ice localized crushing behavior and panel interaction, with the ice sphere volume away from the crushed zone (at the sphere-panel interface) maintaining a mostly hemispherical shape. This localized crushing was also observed in models predicting ice impact forces during impact onto rigid targets [Tippmann, Kim and Rhymer (2013)] prior to the ice sphere volume failing more globally.

In the FEA "numerical experiments", the failure threshold limits were identified iteratively by running the model at a starting velocity near the expected FTV. If no damage was indicated by the separation of the cohesive elements, then the velocity was increased. If damage was predicted, then the velocity was decreased. These "numerical experiments" were repeated until bounding velocities within a 5 m/s range were determined. These bounding velocities were then averaged to obtain the FTV FEA values shown in Table 3. Compared to the experimentally-measured values, the FTV FEA predictions were within a range of 1 to 27%, with greater under-prediction of FTV occurring more for the thinner panels and for larger-radius SHI. Under-prediction of FTV can be considered as conservative, as the models predict damage initiation at lower than actual velocities. Rationale for the under-prediction is provided in the following section.

It should be emphasized that the FTV FEA values were determined independently of the experimental FTV values via the "numerical experiment" process just described. Note that numerical results for the 24 ply panel impacted by 38.1 mm SHI were not obtained due to numerical instabilities at this condition, preventing successful completion of the model runs. The analysis unexpectedly terminated due to select elements located on the impact side at ∼10 mm from the panel center (along both symmetry planes) exhibiting non-physical deformation states as a result of high local contact stresses created during very high velocity impact (over 200 m/s). Although the 24 ply panel with 38.1 mm SHI results were not available, the absence of these results does not affect the findings and conclusions.

In addition to the FTV, the FEA models predicted the contact force histories during impact. Figures 8, 9, and 10 show the 8, 16, and 24 ply force histories, respectively, for the numerically-determined impact velocities that bound the FTV within the 5 m/s range. The star markers shown on the upper bound plots indicate when the first cohesive element fails. This force level, defined as the critical force associated with the onset of damage initiation, is summarized in Table 3 for each case. The critical force occurs near the time of peak force of the impact, sometimes prior to the peak force as the critical value is achieved during the force build up, and often after the peak force as it takes a small amount of time for the interlaminar shear stresses to build up and fail an entire cohesive element. The initial cohesive
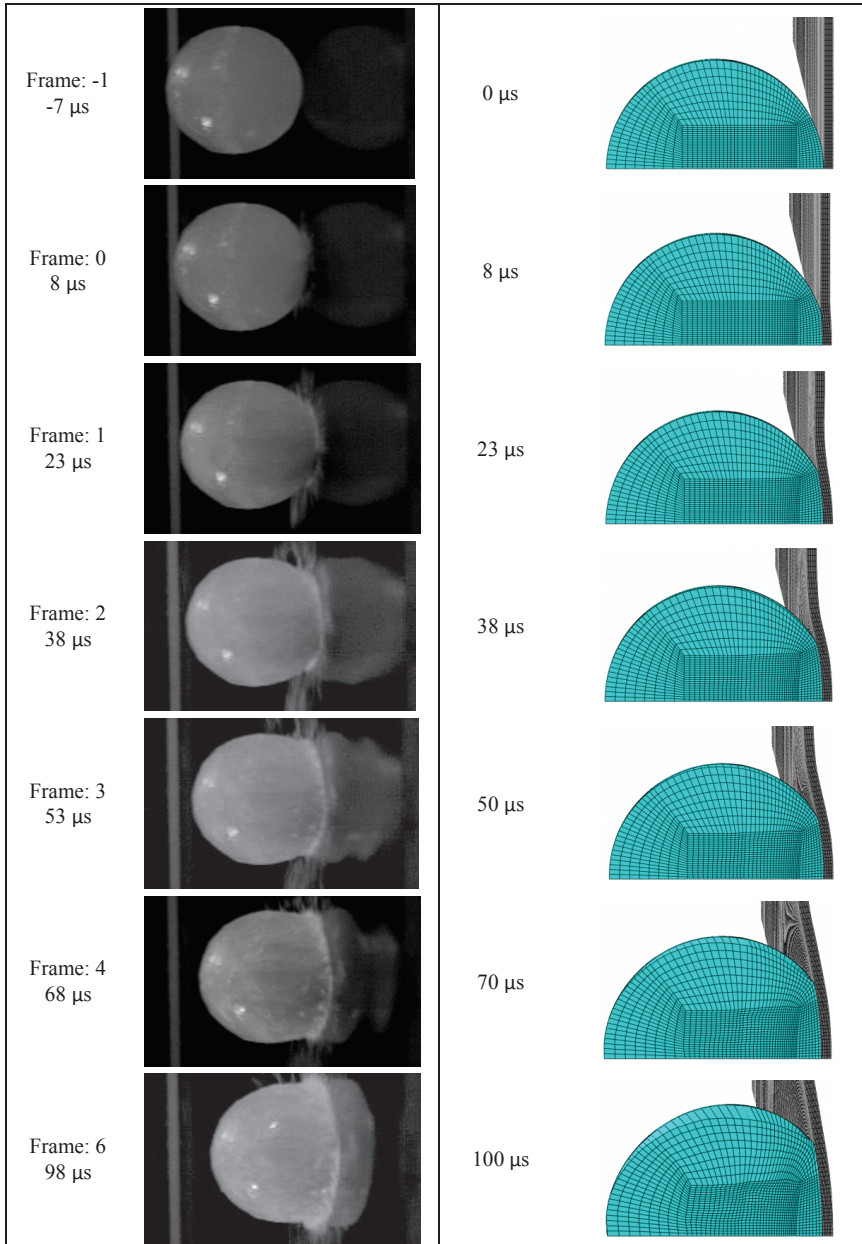
Figure 7: Comparison of Predicted and Experimentally-Observed Deformations of 38.1 *mm* SHI Impacting 8 Ply Panel at 126 *m/s*
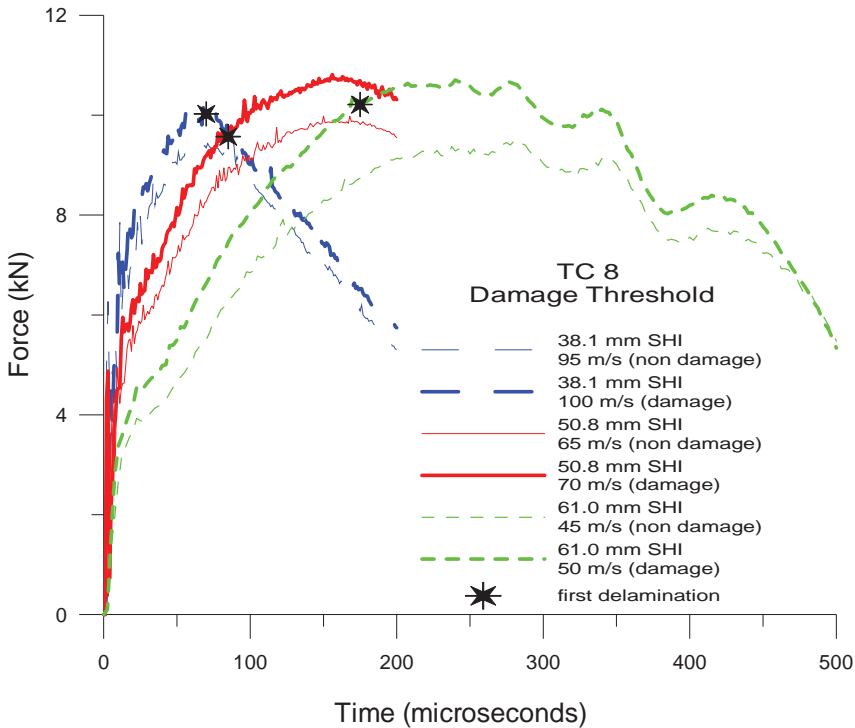
Figure 8: Force Histories for the Bounding Velocities of 8 Ply Panels

element to fail is usually located at a small distance away from the panel center, as shown by the deleted elements in Figure 11 where only the 6th cohesive element layer is shown (i.e., the planar interface between the 6th and 7th plies from the impact side). Ideally, the exact threshold velocity, not an average of bounds, would have found the critical force and peak force coincident to each other.

Of particular interest is the (non-intuitive) observation that the critical force is essentially the same for each panel thickness, despite the different SHI diameters and velocities. In order to achieve the same force level, a smaller diameter SHI must impact the panel at higher velocity. Increasing panel thickness requires higher critical force to initiate damage, which is reflected in last column of Table 3 showing higher velocity needed for a given SHI diameter to initiate damage in thicker panels. At velocities higher than the FTV, the FEA models predict more extensive delamination area. As an example, Figure 12 shows the deleted elements of an 8 ply panel's 4th cohesive element layer (located at the panel midplane, i.e., the interface between the 4th and 5th plies) which represents the extent of delamination
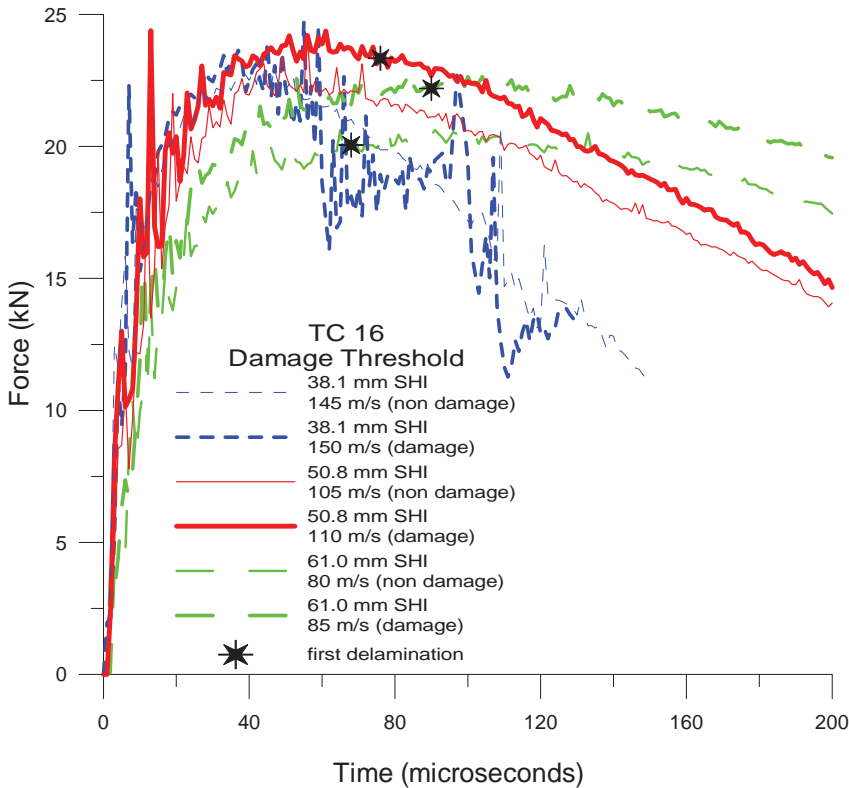
Figure 9: Force Histories for the Bounding Velocities of 16 Ply Panels

produced by this impact.

A 24 ply panel having three strain gages (see Figure 3) was impacted with 50.8 *mm* SHI. Figure 13 shows a plot of the history response all three strain gages for 116 *m/s* impact onto the 24 ply panel. These strain gage data provide response information that can be used to verify the accuracy of the FEA models. A high level of strain was developed (8,000 microstrain) at the center of the panel, with lower peak strains measured at 70 *mm* distance from panel center in the 0 and 90 degree directions. The verification of the panel models was demonstrated by comparing the predicted strain response with the measured data. Figure 13 shows the FEA model has a slightly higher strain value for the center and 90 degree gages, but otherwise matches the strain response (history shape) well. The FEA did not predict the 70 *mm* offset 0 degree gage magnitude properly, however, and this might be due to targeting error of the ice sphere (actual impact location not at center). The higher predicted peak center strain is consistent with the fact that the simulated ice
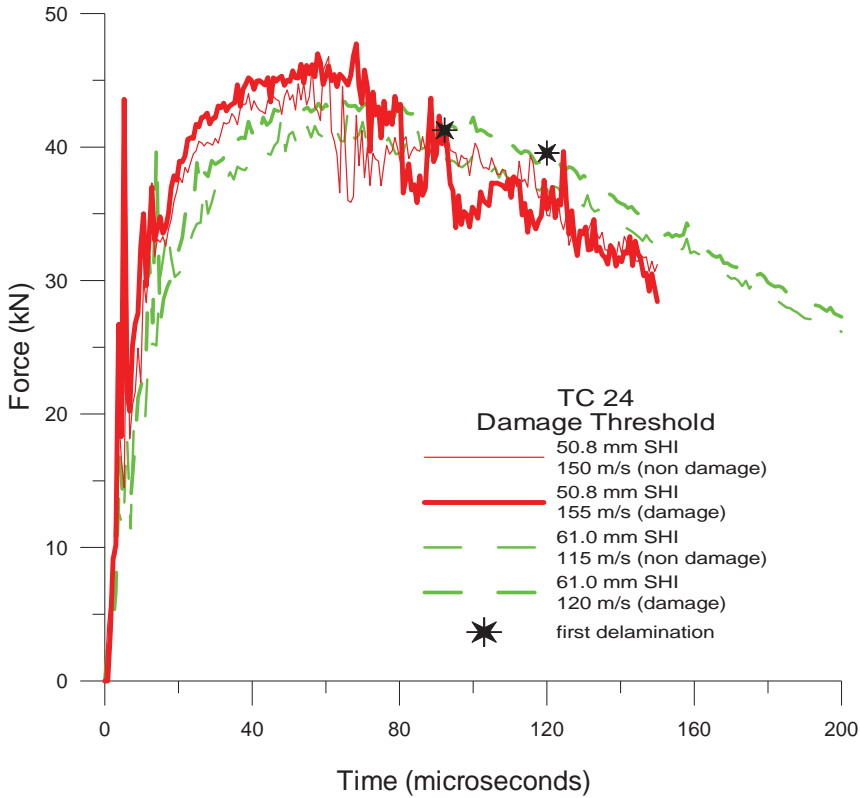
Figure 10: Force Histories for the Bounding Velocities of 24 Ply Panels

material model [Tippmann, Kim and Rhymer (2013)] represents the strongest ice, compared to the average experimental ice, and therefore produced slightly larger strain results.

5   Model Correlation

The experimentally and numerically determined FTV were established independently of each other, with the FEA model velocity adjusted up and down to find the onset of failure, mirroring the procedure followed in the experiments [Rhymer, Kim and Roach (2012)]. The FEA model is deemed to be predictive since no "tuning" of the composite or ice material properties, or of the cohesive zone strength and fracture properties, was done in seeking better experimental correlation. An available set of known (published) values were used in defining the composite [Swanson and Qian (1992); Yokozeki, Ogasawara and Ishikawa (2006); Takeda,
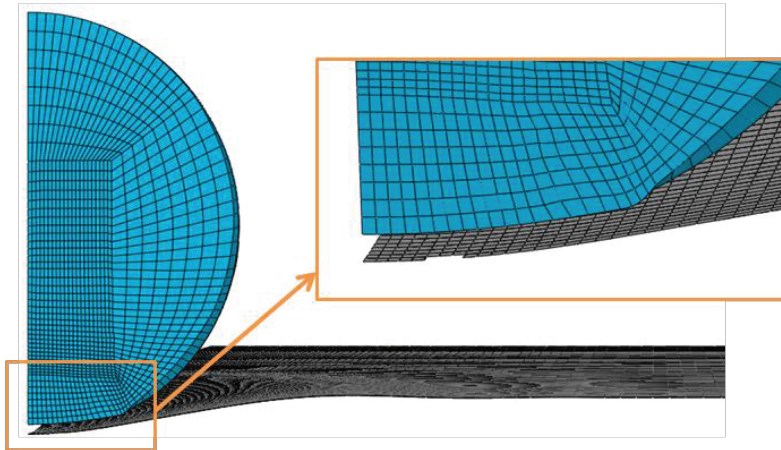
Figure 11: Elements Deleted From 6th Cohesive Element Layer (at Interface Between 6th and 7th Plies) Corresponding to Damage Initiation for 50.8 *mm* SHI Impact of 8 Ply Panel at 70 *m/s*
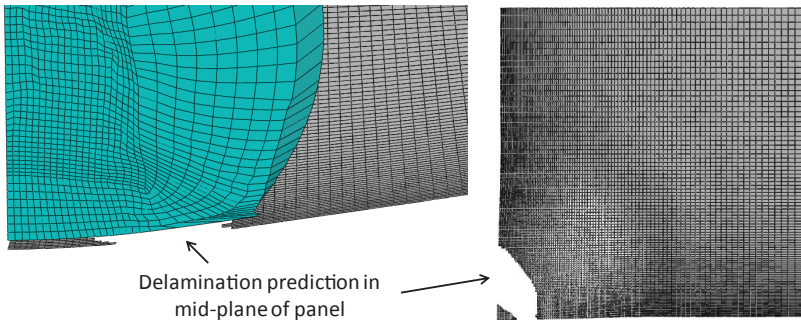

Figure 12: Elements Deleted From 4th Cohesive Element Layer (at Interface Between 4th and 5th Plies) Showing Extent of Delamination Resulting from 50.8 *mm* SHI Impact of 8 Ply Panel at 95 *m/s* (1.35xFTV)

Kobayashi, Ogihara and Kobayashi (1999); Davidson and Sediles (2011); Hojo, Matsuda, Tanaka, Ochiai and Murakami (2006)], and an established formulation of the ice model [Tippmann, Kim and Rhymer (2013)] was used which was based on rate-dependent strength data [Kim and Kuene (2007)].

All predicted FTV are lower than the experimental values. This is in part due to the ice model having been defined to represent the strongest ice (fitting to top of scatter in measured strength [Tippmann, Kim and Rhymer (2013); Kim and Kuene
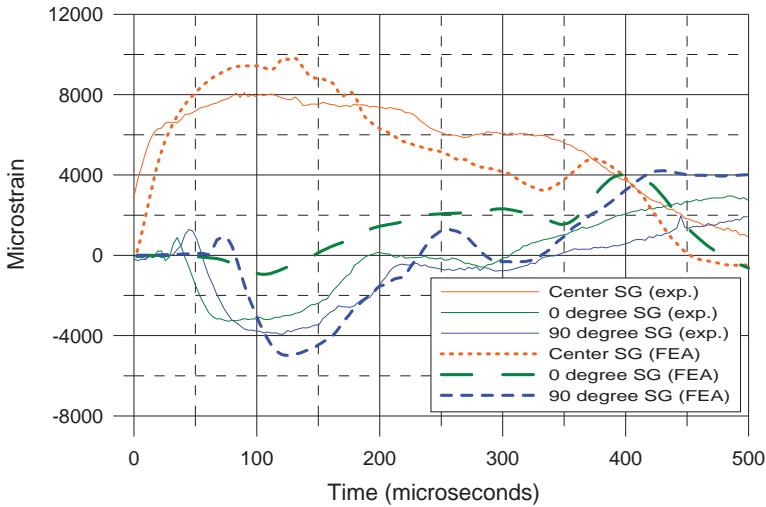
Figure 13: Strain Comparison, 24 ply Panel Impacted by 50.8 *mm* SHI at 116 *m/s*

(2007)]) and therefore a given impacting velocity would produce higher contact forces resulting in a lower predicted FTV, compared to if the model represented the average ice strength data. Furthermore, predictions were found to be more accurate for stiffer (thicker) panels and for smaller diameters (implying higher velocities). Both of these factors result in the ice sphere exhibiting more crushing behavior. Higher level of ice crushing can be associated with improved accuracy due to the fact that the ice model was developed and validated for impacts onto a "rigid" surface which induces more local failure/crushing of the ice sphere than for impacts onto flexible composite panels.

The panel thickness has a strong influence on the mismatch in predicted FTV, which can be related to three aspects: i) Fewer solid elements have more difficulty in accurately predicting higher through-thickness stress gradients in the thinner panels (recall each ply modeled with one layer of solid elements). ii) The choice of quarter-symmetry for modeling the panels is a source of modeling error, particularly for the 8 ply panels since they exhibit bend-twist coupling. Specifically, the D_{16} and D_{26} terms in the Classical Laminated Plate Theory bending stiffness $[D]$ matrix are 9.7% of D_{11} for the 8 ply panels (see Table 4). The coupling is much less in the 16 and 24 ply panels, at 3.4% and 1.6% of D_{11}, respectively (see Table 4). Quarter-symmetry imposes additional constraint to the problem and so the 8 ply panels will exhibit higher stiffness, compared to no symmetry being imposed (i.e., full-plate FEA model). Thus, modeling the full panel would likely produce higher

predicted FTV values (i.e., a better match to experiments) for the 8 ply panels since the more compliant full model (no symmetry) would need higher velocity to achieve a given impact-contact force level. The use of quarter-symmetry to reduce model size was required, however, in order to be able to completed each model's calculations in a

reasonable time (several days per model run). (iii) The material properties used to model the T800/3900-2 composite [Tong and Soutis (2003); Swanson and Qian (1992); Yokozeki, Ogasawara and Ishikawa (2006); Takeda, Kobayashi, Ogihara and Kobayashi (1999); Davidson and Sediles (2011); Hojo, Matsuda, Tanaka, Ochiai and Murakami (2006)] plies were measured under quasi-static loading rates. Interlaminar fracture behavior is known to exhibit strain rate sensitivity, and thus accounting for this dependency could possibly improve the experimental correlation since higher strain rates are typically associated with higher measured interlaminar strength properties [Cantwell (1997)]. Fiber-dominated properties can also exhibit rate sensitivity, although more strongly observed for glass fibers [Marguet, Rozycki and Gornet (2006)] than for carbon. Finally, it should be noted that the plies were modeled as elastic without failure. Even when no fiber failure occurs, matrix cracking is known to develop which can cause local softening and propagate to ply interfaces, thereby initiating delamination.

Table 4: Laminate Bending Stiffness Matrix Terms and Effective Bending Stiffness D^*

Panel Type (Thickness)	D_{11} $(N \cdot m)$	D_{12} $(N \cdot m)$	D_{22} $(N \cdot m)$	D_{66} $(N \cdot m)$	$D_{16} = D_{26}$ $(N \cdot m)$	D^* $(N \cdot m)$
8 ply (1.59 mm)	34.9	4.29	12.3	5.47	3.40	19.3
16 ply (3.11 mm)	199	46.9	153	56.3	6.81	171
24 ply (4.66 mm)	621	166	553	198	10.2	580

The black stars in Figures 7 to 9 indicate the first occurrence of cohesive element failure, i.e., all four integration points of a single cohesive element have failed. This initial delamination developed near the back face of the panel, at the interface between the 90 and 45 degree plies as shown in Figure 14 for the three different panel thicknesses, and was located a small distance away (3 to 5 *mm*) from the center of the panel, thereby resulting in an off-center delamination zone as shown in Figures 11 and 12. The FEA-predicted off-center delamination shape (e.g., in Figure 12), qualitatively matches with the experimental C-scan results [Rhymer, Kim and Roach (2012)], an example of which is shown in Figure 15. It should be noted, however, that the quarter-symmetry assumption predicts the delamination

shape in Figure 12 to be repeated in the other three quadrants, while in actuality, the resulting delamination should be unsymmetric as shown in Figure 15.
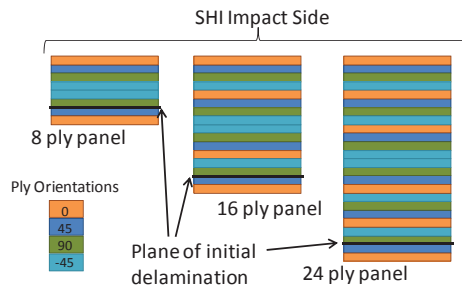

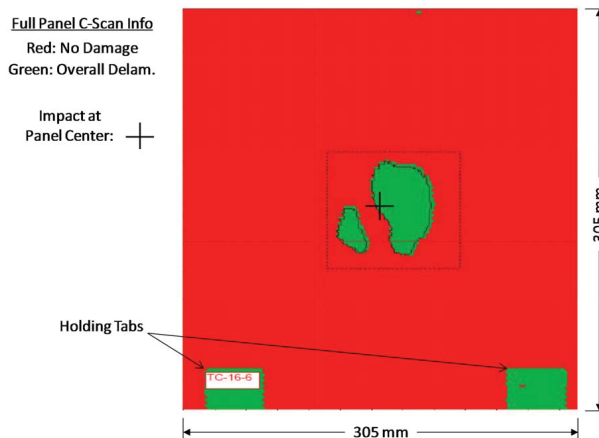Figure 14: FEA Damage Initiation Plane in Panels

Figure 15: Delamination Shape Near FTE for 16 Ply Panel Impacted With 38.1 *mm* SHI at 162 *m/s*; Green Color Indicates Overall Delamination Existing at Any Plane Within the Laminate, Red Color Indicates No Delamination

6   Critical Force as Simple Failure Criterion

The critical forces associated with the threshold velocity (FTV) were found using FEA. These contact force data were not readily measurable during the experiments involving high velocity projectiles which crush during the impact event. Critical force was unique for each panel thickness tested, but did not change (significantly)

with the variation of SHI diameter. These particular FEA models were computa-
tionally expensive due to their layer-by-layer solid element construction with co-
hesive elements located between each layer of solids. Therefore, a less expensive,
simpler, design-oriented extension of these FEA results is desired as it would be
more widely useful. Thus, a simplified damage initiation prediction capability was
sought based on the critical force concept. It was observed that the critical force
increases as a strong function of panel thickness (see Table 3). The relationship
is material and layup dependent, and thus in an effort to generalize the results, an
effective panel bending stiffness description, D^*, developed by Olsson, Donadon
and Falzon (2006) and shown in Equations (5) and (6), was adopted to more gen-
erally describe the impacted panel's material, layup, and thickness information via
a single parameter.

$$D^* = \left[D_{11}D_{22}\frac{\eta+1}{2} \right]^{1/2} \tag{5}$$

where

$$\eta = \frac{D_{12}+2D_{66}}{(D_{11}D_{22})^{1/2}} \tag{6}$$

In these equations, the terms D_{11}, D_{22}, D_{12} and D_{66} are the terms of the bending
stiffness matrix of an (assumed) orthotropic panel, as described by Classical Lam-
inated Plate Theory. The values for D_{ij} and D^* for each panel type are provided in
Table 4. The critical force was found to scale linearly with respect to $(D^*)^{1/2}$ as
shown in Figure 16. This square root relationship is based on insight gained from
Olsson, Donadon and Falzon (2006) and will be discussed below. If the peak force
of an impact was known, conceivably from a less computationally expensive model
(e.g., shell elements modeling target structure, or even using analytic models), this
relationship can be used to estimate whether damage has occurred in a compos-
ite panel having similar interlaminar shear strength and quasi-isotropic type layup,
when impacted by SHI.

Figure 16 is modified by relating the critical force to associated FTV to produce
Figure 17, which plots the product of the projectile diameter d and the FEA-
predicted failure threshold velocity V_{FTE} versus $(D^*)^{1/2}$. Ice diameter and velocity
are quantities that define the impact threat and are typically known for an impact
event. These are often specified as requirements against which structures must
show resistance to failure (e.g., withstand impact from 50.8 *mm* hail ice at 150 *m/s*
with no damage), and thus Figure 17 provides a design-oriented damage prediction
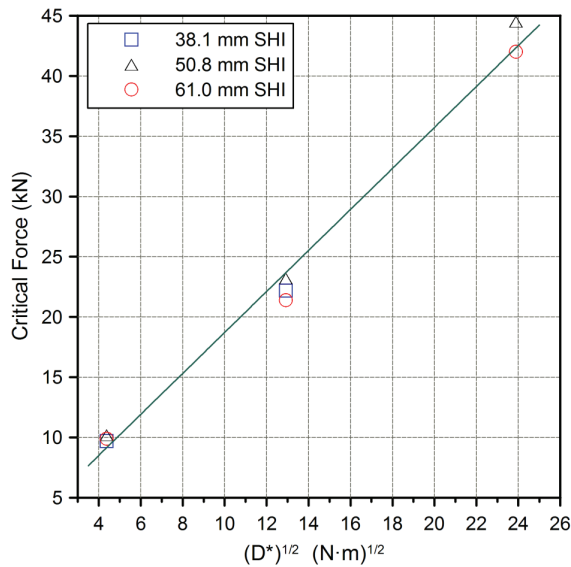capability based on three known key parameters: ice diameter, velocity, and panel

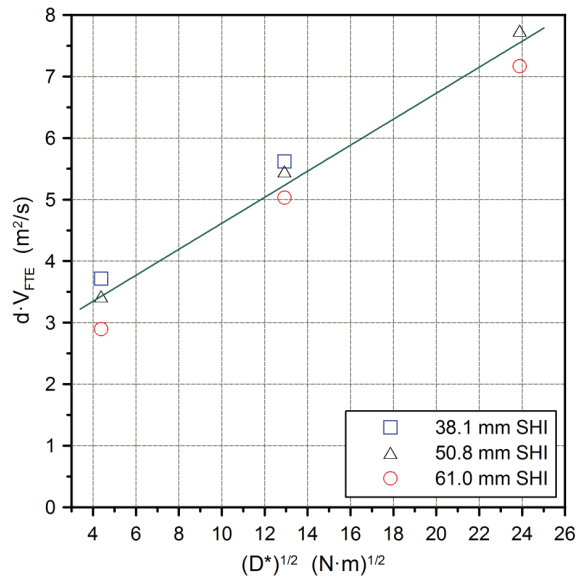Figure 16: Critical Force Versus Effective Bending Stiffness

Figure 17: SHI Diameter Times Critical Velocity Versus Effective Bending Stiffness

effective bending stiffness (embodies material stiffness, thickness, and layup information). Additionally, this plot can be used as a tool for establishing the minimum diameter for which an impacted aircraft skin would require inspection following a hailstorm of known falling ice diameter and assumed impact velocity (terminal falling velocity+wind gust). The applicability of the results in Figures 16 and 17 extends generally to toughened carbon/epoxy composite materials having a similar level of interlaminar strength (see values in Table 2) and having quasi-isotropic type layup, since the interlaminar strengths are the key material properties related to delamination. This statement is corroborated by the overlap of V_{FTE} data for laminates made from unidirectional plies of T800/3900-2 material and woven plies of AS4/977 and AS4/8552 (i.e., different material), as reported by Rhymer, Kim and Roach (2012). In the referenced work, two very different lamina materials (uni vs. woven) exhibited the same failure threshold response to ice sphere impact. Both resin systems were toughened epoxy and had similar interlaminar shear strength.

To generalize further the results in Figures 16 and 17, the work of Olsson, Donadon and Falzon (2006) was used which predicts the delamination threshold force (critical force) for a small mass high velocity impact:

$$F = C\pi\sqrt{\frac{32}{3}G_{IIC}D^*} \tag{7}$$

where C is the dynamic scaling term

$$C \approx \frac{1}{\sqrt{1 - \frac{7\pi^2}{216}}} = 1.213 \tag{8}$$

Note that Equation (7) developed by Olsson, Donadon and Falzon (2006) considers the projectile-panel interaction as a concentrated load, and thus is only dependent on two variables: D^* (previously defined) and G_{IIC}, which is the critical strain energy release rate for mode II interlaminar fracture of the composite.

An investigation was conducted to extend the applicability of Equation (7), developed for small rigid spherical projectile, to high velocity ice sphere impact which locally crushes and thus involves a relatively larger contact area. Figure 18 plots the critical force calculated by Equation (7) as a function of $(D^*)^{1/2}$ for $G_{IIC} = 2200 \ J/m^2$ (per Table 2). This appears as the lowest curve in the figure labeled "Point Load". As Juntikka and Olsson (2009) stated, this equation does not represent high velocity ice impacts, which can be seen by comparing the "point load" line to the FEA-determined critical force data points also plotted in Figure 18. This is due to the ice impact developing a much larger contact area than the point load assumed in Equation (7). However, Equation (7) does represent the correct
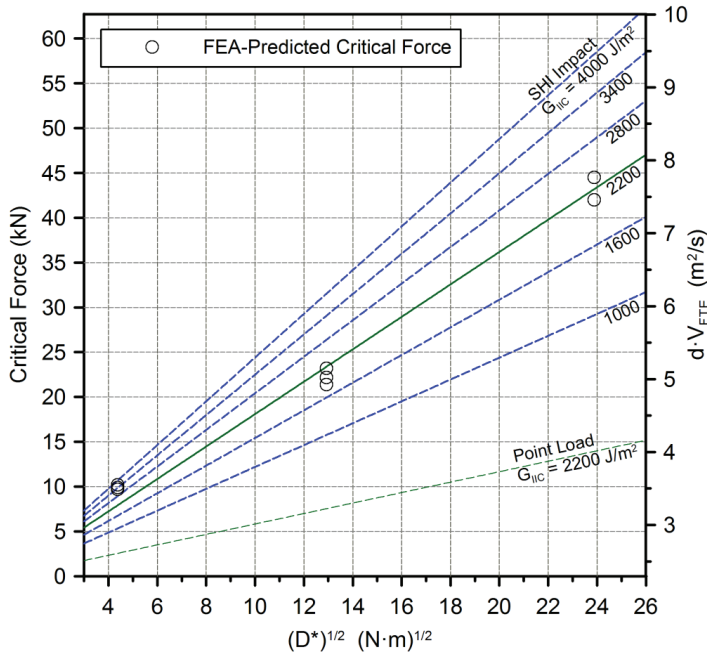
Figure 18: Scaling of Critical Force with Interlaminar Properties and Effective Bending Stiffness; Mapping Between Vertical Axes via ($dV_{FTE} = 0.123 F_{crit} + 2.29$ (Linear Fit, $R^2 = 0.95$)

general trend of the data points (linear with respect to square root of D^*), and thus can be considered to properly represent the physics of the delamination initiation. To account for the increased projectile contact area (which is dependent on the projectile material and geometry for small displacements in the panel), a contact area scaling constant k was added to Equation (7), yielding Equation (9).

$$F = kC\pi\sqrt{\frac{32}{3}G_{IIC}D^*} \tag{9}$$

where $k = 3.1$ was found to best match the data (curve fit) for all three panel types, and can thus be considered representative for ice spheres contacting composite panels of widely-varying stiffness. The constant k is primarily projectile dependent (material and geometry) and would need to be reassessed for other projectile types, e.g., rubber debris.

The prediction of Equation (9) plotted in Figure 18 for $G_{IIC} = 2200 \, J/m^2$ shows

a close match to the data points, with better matchup found for the higher stiffness (thicker) panels. The curve corresponding to $G_{IIC} = 2200 \ J/m^2$ provides a prediction capability for the critical force leading to initiation of delamination in composite panels having this particular value of G_{IIC}. To explore the sensitivity of critical force to the variation in G_{IIC}, the G_{IIC} value was adjusted to create a set of design-oriented curves, plotted in Figure 18, for G_{IIC} values spanning a realistic range typical of polymer matrix composite materials. The results in Figure 18 can now be considered as generally applicable to predicting the critical force associated with delamination initiation for high velocity ice sphere impacts onto a variety of composite panels having quasi-isotropic type layup (i.e. has 0, ±45, and 90 fiber orientations). Key parameters are the panel's effective bending rigidity D^* and the mode II interlaminar critical strain energy release rate G_{IIC}. A second vertical axis was added to Figure 18, mapping the critical force to the product of ice diameter and the failure threshold velocity. In this form, the results in Figure 18 can be used, as described earlier, for sizing skins to be resistant to ice sphere impacts.

Knowing the critical force, as predicted by Equation (9), allows for more simplified models to be employed to investigate ice impacts. Specifically, models representing the stiffness and dynamic response interaction between the ice sphere and impacted structure that can accurately predict the force time history will typically be less computationally expensive than detailed layer-by-layer solid models which enable interlaminar stress prediction. Addition of cohesive zone elements between the solid element layers adds to the computational expense, and such modeling approach is not conducive to simulating the impact of larger-sized structures (e.g., an aircraft wing). Computational cost can be dramatically reduced by representing the through-thickness direction of the panel with laminated shell elements, with the aim of accurately predicting the contact force history during the impact event.

Figure 19 is a plot of the force histories predicted for SHI impacts onto solid and shell element models of the 16 ply composite panels at the experimentally-determined critical velocities. Despite the shell models not explicitly simulating delamination, the force histories of the shell element based models (dashed lines) match the histories predicted by solid element models (solid lines) quite closely.

Since critical force can be used as a key parameter for delamination onset prediction, this demonstrates the viability of using shell-based models for representing larger structures of interest, where the primary output of interest would be an estimate of the contact force history. Many large-sized structures, such as a full aircraft, require the use of shell models from a computational cost viewpoint. This modeling approach will only be applicable to predicting the onset of damage, and not the extent, since the shell elements (as implemented) lack any representation of damage-formation.
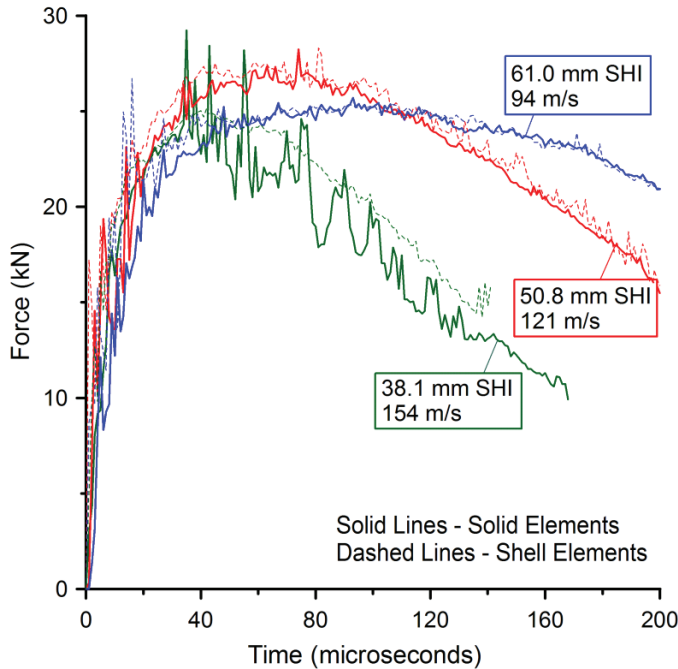
Figure 19: Comparison of Force Histories for Shell Element and Solid Element Models of 16 Ply Panels

7   Conclusion

A modeling approach has been demonstrated for predicting the onset of delamination damage in carbon/epoxy panels impacted by high velocity ice spheres. The FEA model described in this paper is considered to be predictive, since the panel material properties are all based upon values found in the literature for this material system, and no material parameters were tuned to match the experimental results. The models have been used to determine the critical force level at which damage onset occurs, associated with each panel thickness. The critical force was found to be independent of the ice projectile diameter. Such an observation provides the basis for establishing a threshold critical force failure criterion that would define the initiation of damage in a manner that is independent of the ice projectile diameter. Alternative simulations (e.g., shell elements or reduced order analytical models) could conceivably be used in conjunction with this critical force damage initiation criterion to predict the onset of delamination without using computationally expensive solid elements and cohesive zone elements. Design-oriented curves were established between key parameters, which include the ice diameter and velocity

(defines impact threat), the panel effective bending stiffness, and interlaminar fracture energy G_{II_c}. This relationship can be used for skin sizing by establishing minimum gage skin thickness (of quasi-isotropic type laminates) based on hail impact requirements, or for making threat assessment of an already established laminate design.

References

Cantwell, W. J. (1997): The influence of loading rate on the mode II interlaminar fracture toughness of composite materials. *Journal of Composite Materials*, vol. 31, no. 14, pp. 1364–1380.

Dassault Systèmes Simulia Corp (2011): *ABAQUS v.6.11 Analysis User's Manual*. Dassault Systèmes Simulia Corp., Providence, RI, USA.

Davidson, B. D.; Sediles, F. O. (2011): Mixed-mode I-II-III delamination toughness determination via a shear-torsion-bending test. *Composites Part A: Applied Science and Manufacturing*, vol. 42, no. 6, pp. 589–603.

Davies, G. A. O.; Zhang, X. (1995): Impact damage prediction in carbon composite structures. *International Journal of Impact Engineering*, vol. 16, no. 1, pp. 149–70.

Elmarakbi, A. M.; Hu, N.; Fukunaga, H. (2009): Finite element simulation of delamination growth in composite materials using LS-DYNA. *Composites Science and Technology*, vol. 69, no. 14, pp. 2383–2391.

Gonzalez, E. V.; Maimi, P.; Turon, A.; Camanho, P. P.; Renhart, J. (2009): Simulation of delamination by means of cohesive elements using an explicit finite element code. *CMC: Computers, Materials, and Continua*, vol. 9, no. 1, pp. 51–92.

Hojo, M.; Matsuda, S.; Tanaka, M.; Ochiai, S.; Murakami, A. (2006): Mode I delamination fatigue properties of interlayer-toughened cf/epoxy laminates. *Composite Science and Technology*, vol. 66, no. 5, pp. 665–75.

Jackson, W. C.; Poe, C. (1992): The use of impact force as a scale parameter for the impact response of composite laminates. Technical Report AVSCOM Technical Report 92-B-001, NASA Technical Memorandum 104189, 1992.

Juntikka, R.; Olsson, R. (2009):   Experimental and modeling study of hail impact on composite plates. In *Proceedings of the 17th International Conference on Composite Materials*, Edinburgh, Scotland UK.

Kim, H.; Kedward, K. T. (2000):   Modeling hail ice impacts and predicting impact damage initiation in composite structures. *AIAA Journal*, vol. 38, no. 7, pp. 1278–88.

Kim, H.; Kuene, J. N. (2007):   Compressive strength of ice and impact strain rates. *Journal of Material Science*, vol. 42, no. 8, pp. 2802–806.

Kim, H.; Welch, D. A.; Kedward, K. T. (2003):   Experimental investigation of high velocity ice impacts on woven carbon/epoxy composite panels. *Composites Part A: Applied Science and Manufacturing*, vol. 34, pp. 25–41.

Marguet, S.; Rozycki, P.; Gornet, L. (2006):   Rate dependent constitutive model for glass-fibre / epoxy-matrix woven fabrics. *CMC: Computers, Materials, and Continua*, vol. 4, no. 3, pp. 119–136.

Olsson, R. (2010):   Analytical model for delamination growth during small mass impact on plates. *International Journal of Solids and Structures*, vol. 47, no. 21, pp. 2884–92.

Olsson, R.; Donadon, M. V.; Falzon, B. G. (2006):   Delamination threshold load for dynamic impact on plates. *International Journal of Solids and Structures*, vol. 43, no. 10, pp. 3124–41.

Olsson, R.; Juntikka, R. (2010):   Validation of analytical model for hail impact on composite laminates. In *Proceedings of 14th European Conference on Composite Materials*, Budapest, Hungry.

Rhymer, J.; Kim, H. (2010):   High velocity ice impact damage resistance comparison of unidirectional and woven carbon/epoxy composite panels. In *Proceedings of the American Society for Composites: 25th Annual Technical Conference*, Dayton, OH. American Society for Composites.

Rhymer, J.; Kim, H.; Roach, D. (2012):   The damage resistance of quasi-isotropic carbon/epoxy composite tape laminates impacted by high velocity ice. *Composites Part A: Applied Science and Manufacturing*, vol. 43, no. 7, pp. 1134–44.

Schoeppner, G. A.; Abrate, S. (2000):   Delamination threshold loads for low velocity impact on composite laminates. *Composites Part A: Applied Science and Manufacturing*, vol. 31, no. 9, pp. 903–15.

Swanson, S. R.; Qian, Y. (1992):   Multiaxial characterization of T800/3900-2 carbon epoxy composites. *Composite Science and Technology*, vol. 43, no. 2, pp. 197–203.

Takeda, N.; Kobayashi, S.; Ogihara, S.; Kobayashi, A. (1999): Effects of toughened interlaminar layers on fatigue damage progress in quasi-isotropic CFRP laminates. *International Journal of Fatigue*, vol. 21, no. 3, pp. 235–42.

Tippmann, J. D.; Kim, H.; Rhymer, J. D. (2013): Experimentally validated strain rate dependent material model for spherical ice impact simulation. *International Journal of Impact Engineering*, vol. 57, pp. 43–54.

Tong, L.; Soutis, C. (2003): *Recent Advances in Structural Joints and Repairs for Composite Materials*. Springer. Table 4.1, pp 119.

Yokozeki, T.; Ogasawara, T.; Ishikawa, T. (2006): Nonlinear behavior and compressive strength of unidirectional and multidirectional carbon fiber composite laminates. *Composites Part A: Applied Science and Manufacturing*, vol. 37, no. 11, pp. 2069–79.